Chemical Engineering Research and Design 206 (2024) 440–452

Contents lists available at ScienceDirect

Chemical Engineering Research and Design

journal homepage: www.elsevier.com/locate/cherd

Unary adsorption of sulfonamide antibiotics onto pozzolan-tyre ash based geopolymers: Isotherms, kinetics and mechanisms

Hermann Dzoujo Tamaguelon [a], Victor Odhiambo Shikuku [b,*], Sylvain Tome [a], Fidele Gallo Titini [a], Pamela Ondiek [c], Till Strothmann [d], Zachary Getenga [c], Christoph Janiak [d], Marie Annie Etoh [a], David Daniel Joh Dina [a]

[a] Department of Chemistry, Faculty of Sciences, University of Douala, P.O. Box 24157, Douala, Cameroon
[b] Department of Physical Sciences, Kaimosi Friends University, P.O. Box 385-50309, Kaimosi, Kenya
[c] Department of Physical Sciences, Machakos University, P.O. Box 136-90100, Machakos, Kenya
[d] Institut für Anorganische Chemie und Strukturchemie, Universität Düsseldorf, Universitätsstr, Düsseldorf 1D-40225, Germany

ARTICLE INFO

Keywords:
Adsorption
Geopolymers
Tyre ash
Pozzolan
Sulfadimethoxine
Sulfamethoxazole

ABSTRACT

In this contribution, geopolymer composites, GP_0, $GP_{5\text{-}TA}$ and $GP_{10\text{-}TA}$, were prepared by alkaline activation and substituting pozzolan (Pz) with 0, 5 and 10 wt% of tyre ash (TA), respectively. The geopolymers were characterized using standard methods (XRD, TGA, FTIR, BET, SEM, Boehm titration and methylene blue and iodine indices) and were applied for the abatement of two sulfonamides, sulfamethoxazole (SMX) and sulfadimethoxine (SDM) in single-solute solutions. The effects of pH, salinity, initial concentration and contact time were evaluated. The incorporation of 5 and 10% TA increased the specific surface area (SSA) of pristine geopolymer (GP_0) from 13.62 to 21.48 and 29.70 $m^2.g^{-1}$, respectively. The equilibrium data was best described by the Sips isotherm model. Salinity significantly diminished the adsorption of SMX and SDM. In aqueous medium, the geopolymers exhibited higher adsorption capacity for SDM (log K_{ow}, 1.17) relative to SMX (log K_{ow}, 0.86). In contrast, in saline medium, SMX uptake was higher, suggesting a cation-mediated adsorption. Adsorption of SMX was uncharacteristically independent of pH, whereas SDM uptake was significantly pH-dependent. The $GP_{5\text{-}TA}$ geopolymer composite exhibited the highest adsorption capacity for SMX in a saline environment (46.69 $mg.g^{-1}$) and for SDM in non-saline water (107.69 $mg.g^{-1}$). Adsorption rate was described by the pseudo-second order kinetic law. Adsorption mechanism was multi-mechanistic involving hydrophobic, ion exchange and charge assisted hydrogen bonding and electrostatic interactions in the case of SDM. Future works should optimize the functional groups density of active sites especially for sulfonamides in saline waters.

1. Introduction

During the last decades, environmental pollution through indiscriminate discharge of industrial and hospital effluents containing dyes, micronutrients, viruses, microplastics, heavy metals and pharmaceuticals and personal care products (PPCPs), among other pollutants, has been on the rise. Antibiotics are among the most widely used pharmaceutical products for the prevention and treatment of humans, animals and plant infections and to promote animal growth in agriculture and aquaculture (Yang et al., 2019). Antibiotics can thus be released into the environment through various routes such as flushing of old prescriptions, hospital waste, and wastewater treatment plant (WWTP) effluent (Chebii et al., 2024; Ngeno et al., 2023). The presence of antibiotics in terrestrial and aquatic ecosystems has become a major concern due to the acute and chronic effects of antibiotics on ecosystems, including genotoxicity, the proliferation of antibiotic resistant bacteria (ARB) and antibiotic resistant genes (ARG) among other histopathological changes (Li et al., 2018; Zhou et al., 2021). Sulfonamides (SA) is a large group of bacteriostatic antibiotics most frequently detected in surface water, groundwater, sediment, and soil (Chen and Xie, 2018). Unfortunately, these compounds are recalcitrant to traditional WWTP processes due to their chemical stability (Guo and Wang, 2019). Consequently, much research has been focused on developing alternative water treatment technologies to more effectively remove trace antibiotic residues. Adsorption technology on activated carbons (Guo and Wang, 2019; Njewa and Shikuku, 2023), biochars

* Corresponding author.
E-mail address: vshikuku@kafu.ac.ke (V.O. Shikuku).

https://doi.org/10.1016/j.cherd.2024.05.009
Received 11 January 2024; Received in revised form 30 April 2024; Accepted 6 May 2024
Available online 14 May 2024
0263-8762/© 2024 Institution of Chemical Engineers. Published by Elsevier Ltd. All rights are reserved, including those for text and data mining, AI training, and similar technologies.

(Jemutai-kimosop et al., 2022), chelating phosphonic cellulose (Yang et al., 2019), clay minerals (Shikuku et al., 2018), diatomaceous earth (Jemutai-Kimosop et al., 2019), aged microplastics, and magnetic carbon composites (Saucier et al., 2017), among others, has proven to be a promising method for the removal of trace antibiotics from water. However, the inaccessibility in most regions and associated cost of production of most of these adsorbents restricts their widespread adoption, especially for third world countries. The high cost of regeneration of exhausted activated carbons and the substantial loss in adsorption capacity also limit the widespread use of activated carbons (Taquieteu et al., 2023).

Geopolymers are emerging low-cost aluminosilicate adsorbents produced from industrial wastes such as incinerator ashes (Owino et al., 2023) and local natural resources such as fly ash, volcanic ash, pozzolan and laterite by alkalinization or acid activation (Tome et al., 2023a). Recent works by Dzoujo T et al. (2021), Tome et al. (2021), and Dzoujo Tamaguelon et al. (2022) have shown the efficiency of pozzolan-based eco-adsorbents in retaining dyes in the aqueous phase. Nevertheless, the improvement of the reactivity of pozzolan in alkaline medium and the obtaining of more efficient geoadsorbents requires the augmentation of this precursor with adjuvants such as metakaolin (Shikuku et al., 2022), rice husk ashes and bagasse ashes etc. Ashes have been shown to ameliorate the textural and adsorptive properties of geopolymers (Tome et al., 2023b). However, the performance of the so-generated geopolymer composites vary depending on the source of ash material, fraction by mass, and synthesis conditions. Furthermore, this provides a dual function as industrial ash waste management approach by "hiding" the ash in the geopolymer matrix. In Cameroon, waste tyres are usually pyrolyzed for extraction of iron. However, management of the tyre ashes is an unresolved environmental problem. Studies have shown that tyre ashes are highly carbonaceous imbuing them with high adsorption capacities for heavy metals (Shahrokhi-shahraki et al., 2021), tetracycline (TC) antibiotics (Acosta et al., 2016) and dyes (Mui et al., 2010). However, largescale utilization of tyre ash for water treatment suffers the limitation of secondary pollution due to the composition of tyre ash. The combination of tyre ash with pozzolan presents a plausible means to optimize the adsorptive properties of the geopolymers for antibiotics removal from water with concomitant waste tyres ash management benefits and immobilization of any toxic constituents. The effect of tire ash on the structural, textural, mechanical and morphological properties of geopolymers has not been explored. Furthermore, adsorption is a function of properties of both the adsorbent and adsorbate. Sulfonamides are known to have a wide disparity in structural and chemical properties such as; kinetic diameter, acid-base equilibria, electrostatic potential, hydrophobicity, and dipole moment (polarity). However, the interplay of these properties on the interaction of sulfonamides with geopolymer composites has not been documented. To date, geopolymers have only been examined for adsorption of dyes, metal ions, sulphates, surfactants and pesticides. This paucity of data on the utility of geopolymers for the removal of pharmaceutical ingredients has been flagged in a recent review (Elgarahy et al., 2023). Wang et al. (2022) reported the adsorption of tetracycline onto oleic acid-decorated geopolymer with a maximum adsorption capacity of 645 mg.g^{-1} in saline water. Most recently, Jin et al. (2024) reported 95% removal efficiency of tetracycline by metakaolin based geopolymer in saline water. Adsorption research of antibiotics by geopolymers is still in the formative stages. Furthermore, the existing adsorption studies conducted and plausibly in saline water entail tetracycline, whereas in the real environment, other classes antibiotics such as sulfonamides exist. The role of salinity in the selective removal of sulfonamides by geopolymer materials has not been reported as well. A clear gap therefore exists in our understanding of the synergistic or antagonistic effects adsorbent-adsorbate properties and process conditions on the removal of sulfonamides onto geopolymer-tyre ash composites which cannot be determined *a priori* and probing these gaps present the novelty of the present work. The effect of tire ash (TA) on the textural, structural, chemical composition, and adsorption characteristics of geopolymers derived from pozzolan (P_Z) in the sequestration of sulfonamides (sulfamethoxazole (SMX), and sulfadimethoxine (SDM) from water under various environmental conditions were evaluated and are reported here.

2. Materials and methods

2.1. Chemical reagents

Sulfamethoxazole (SMX, 98% purity), sulfadimethoxine (SDM, 98% purity), acetonitrile (99.9% purity), methanol (99.9% purity), sodium chloride (99. 5%), sodium silicate (96% purity) and sodium hydroxide (98% purity) were obtained from Sigma-Aldrich. All chemicals were used as received without further purification.

2.2. Preparation of geopolymer composites

The red pozzolan (Pz) used in this study was collected in the locality of Mbouroukou (Latitude N 5°03'25'' Longitude E 9°53'32'') in the Moungo department of the Littoral region of Cameroon, while the tyre ash (TA) was collected in a tyre calcination quarry in the city of Douala-Cameroon. The two precursors were crushed, sieved through 100 µm sieve and the resulting powders were washed and at 105°C for 4 h. The geocomposites (Fig. 1) were prepared by mixing the pozzolan powders (40 g) initially substituted with 0, 5 and 10 wt% (0, 2 and 4 g, respectively) of tyre ash with 15.5 g of alkaline activating solution (Na_2SiO_3 + 12 M NaOH with a v/v ratio of 2.4) at a liquid/powder weight ratio = 0.39. The different mixtures were homogenized using a mixer for 10 min and the resulting pastes were then moulded in cylindrical PVC tubes, left to stand for 30 min before being dried in an oven at 60°C for 4 days. The resulting geoadsorbent samples, named GP_0, $GP_{5\text{-}TA}$ and $GP_{10\text{-}TA}$, corresponding to the weight fraction of TA (Table S1, supplementary material), were ground, sieved, and washed to remove excess alkaline activation solution then oven-dried at 105°C for 6 h. The resulting powders were stored in plastic containers before characterization and use for adsorption.

2.3. Material characterization

The different mineralogical phases of the different materials were determined by X-ray diffractometry (XRD). XRD patterns were achieved using an X-ray diffractometer (Bruker, Billerica, MA, USA) in the range 5 and 70° (2θ) with 2 s per step as rate using Cu Kα radiation (λ = 1.54184 Å). The crystalline phases were identified using QualX 2 software. The degree of crystallinity was calculated using Origin 9 software. The percentage of amorphous phase was deduced from the degree of crystallinity. The degradation and thermal behaviour of the different materials were evaluated using a NETZTA NETZSCH TG209F3 TGA (Netzsch, Selb, Germany) apparatus between 30 and 800°C. A 15 mg sample was introduced into alumina crucibles and heated with a heating and cooling rate of 6.0 K min^{-1} under a nitrogen atmosphere (20 mL. min^{-1}) with simultaneous recording of the weight loss data. The functional groups and structural changes of the various materials were determined with a Fourier transform infrared spectrophotometer (Bruker, Billerica, MA, USA) using the KBr method between 400 and 4000 cm^{-1}. This was carried out with a resolution of 2 cm^{-1} and 32 scans using the pellet from each sample. Each pellet was prepared by adding approximately 1.2 mg of the sample to approximately 200 mg of KBr. The morphology and internal microstructure of the samples were visualized using a ZEISS EVO L 15 scanning electron microscope (SEM, Hitachi Ltd., Japan) powered by an accelerating voltage of 20 kV. The specific surface areas from the BET method were determined by nitrogen adsorption at 77 K in a pressure range of p = 10^{-3} bar using a Quantachrome Autosorb 6 equipment (Quantachrome, Odelzhausen, Germany). Iodine and methylene blue indices as described by Hermann et al. (2021) were used to assess microporosity and mesoporosity,

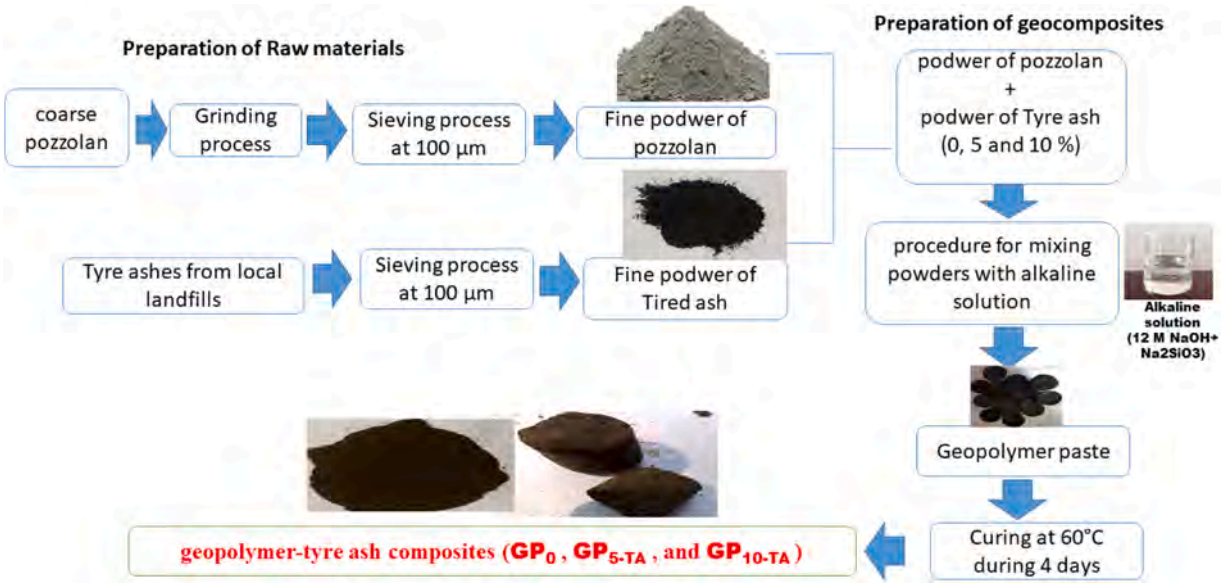

Fig. 1. Schematic diagram on the synthesis of GP-TA geopolymer composites.

respectively. Quantification of the total acidic and basic functional groups present on the surface of the geoadsorbents was determined using the Boehm titration method (Jacques et al., 2023).

2.4. Batch adsorption study

Batch duplicate tests were carried out in 250 mL Erlenmeyer flasks containing 0.05 g of geoadsorbent and 50 mL of a 5 mg/L sulfamethoxazole (SMX) or sulfadimethoxine (SDM) solution. The Erlenmeyer flasks were shaken at 200 rpm for 60 min at 25°C. At predetermined time intervals (30, 60, 90, 120, 150, 120 and 180 min) the residual analyte in the solution was determined. The influence of the initial SMX or SDM concentrations were evaluated in the range 1–5 mg/L. The aliquots were filtered through 0.2 µm syringe filters and the residual SMX and SDM concentrations was determined using HPLC-SHIMADZU (47269 Dulsburg, F.R, Germany) at 268 nm. The mobile phase was a mixture of water (1% acetic acid) and acetonitrile (90:10 v/v), with a flow rate of 1.0 mL/min (Shikuku et al., 2017). The injection volume in the chromatography C18 column was 50 µL. Statistical difference between the mean concentrations of the replicates was determined by analysis of variance (ANOVA) using SAS software at a 95% confidence level. The amount adsorbed at any time t (q_t), adsorption capacity at equilibrium (q_e) and percent removal (%R) were calculated according to Eqs. 1, 2 and 3, respectively.

$$q_t = \frac{(C_i - C_t)V}{m} \quad (1)$$

$$q_e = \frac{(C_i - C_e)V}{m} \quad (2)$$

$$\%R = \frac{(C_i - C_e)}{C_i} \times 100 \quad (3)$$

Where C_i is the initial SMX or SDM concentration, C_t and C_e are the initial concentrations at time *t* and at equilibrium, respectively (mg/L). V is the volume of solution (L) and *m* is the mass of adsorbent (g).

2.4.1. Effect of salinity solution

The tests were performed by initially preparing five 50 mL solutions (1, 2, 3, 4 and 5 mg/L) of SMX or SDM in 0.005 M NaCl solution. A dose of 0.05 g of adsorbent was introduced and stirred until equilibration.

2.4.2. Effect of pH

The effect of pH was examined by varying the pH of the SMX or SDM solution from 2 to 10 using a solution of hydrochloric acid HCl (0.1 N) or caustic soda NaOH (0.1 N) depending on the desired pH.

3. Results and discussion

3.1. XRD analysis

Fig. 2 displays the diffractograms of pozzolan (P_Z), tyre ash (TA)and geoadsorbents and with ($GP_{5\text{-}TA}$) and pristine geopolymer (GP_0). The tyre ash consists of graphite (COD_1100003), Zincite (COD_9004178) and Pyrite (COD_9000594) and 87.75% amorphous phases. The pozzolan contained albite (COD_1556998), anorthoclase (COD_9000856), augite (COD_1000035), clinopyroxene (COD_9005434), magnetite (COD_9000926), feldspar (COD_9000425) and quartz (COD_9012602) as minerals and 21.25% amorphous phases. The minerals initially present in the pozzolan did not disappear after alkalination, reflecting their low dissolution in a alkaline medium. It can also be seen that after activation, the amount of amorphous phase increases slightly, to 27.65% and 32.13% in GP_0 and $GP_{5\text{-}TA}$, respectively. This increase in the amorphous phase is due to the total transformation of the amorphous phase contained in the precursors and a slight transformation of the crystallised aluminosilicates into amorphous polymer, i.e. the geopolymer. The addition of tyre ash also increased the amount of amorphous phase. Tyre ash did not affect the geopolymerization reaction to result in new mineralogical phases. These results are not similar to the work of Dzoujo Tamaguelon et al. (2022) who reported that the integration of biochar into the geopolymeric chain generated a crystalline phase.

3.2. TGA analysis

Fig. 3 shows the thermograms of GP_0, $GP_{5\text{-}TA}$ and $GP_{10\text{-}TA}$ geoadsorbents recorded between 20 and 800°C. From the first degradation phase (a), a first loss of mass is observed at T<100°C of 0.42%, 0.43% and 0.43% respectively for GP_0, $GP_{5\text{-}TA}$ and $GP_{10\text{-}TA}$. This reflects an endothermic dehydration reaction of these different materials (Tome et al., 2021). In the second degradation phase (b) between 100 and 500 °C, mass losses of around 1.79%, 2.38%, and 2.6% for GP_0, $GP_{5\text{-}TA}$, and $GP_{10\text{-}TA}$ respectively are attributable to dehydroxylation reactions (Dzoujo T et al., 2021). Moreover, it is observed from the thermograms

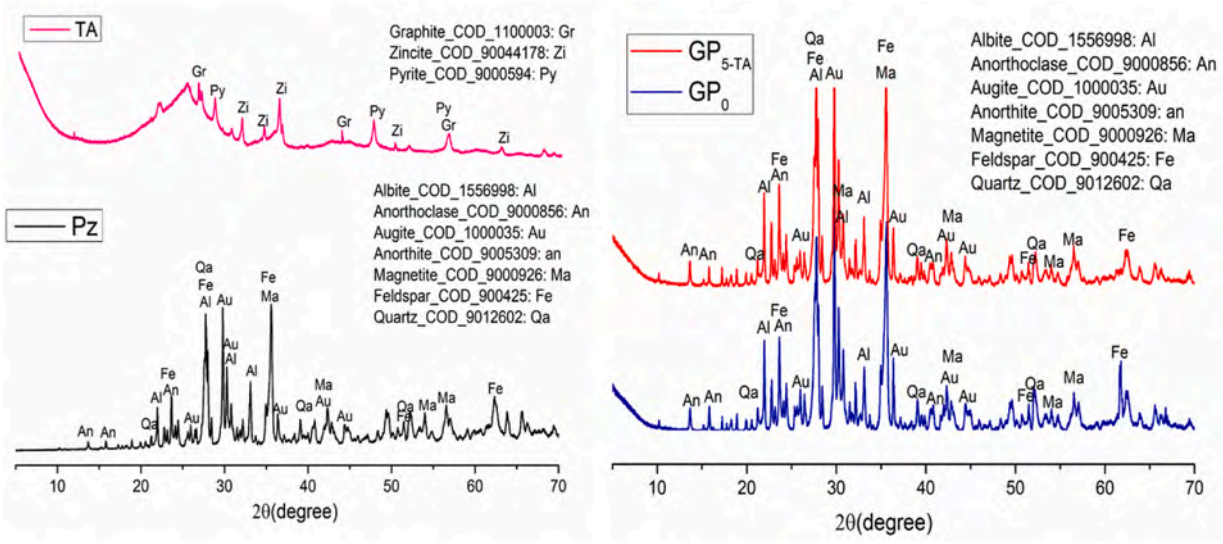

Fig. 2. XRD patterns of pozzolan (Pz), tyre ash (TA) and geoadsorbents and with ($GP_{5\text{-}TA}$) and without (GP_0) tyre ash.

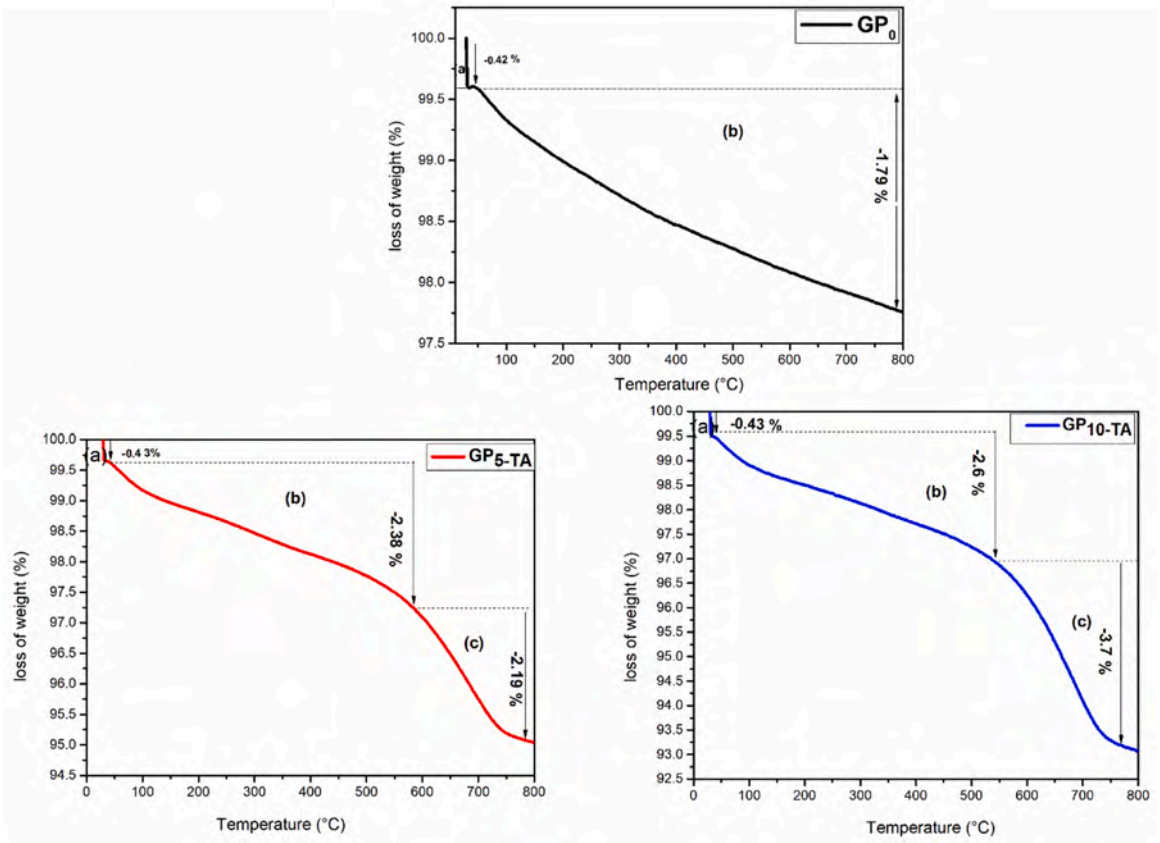

Fig. 3. Different phases of thermal degradation of GP_0, $GP_{5\text{-}TA}$ and $GP_{10\text{-}TA}$ geomaterials.

of the $GP_{5\text{-}TA}$ and $GP_{10\text{-}TA}$ geopolymer composites, contrary to the pristine geopolymer (GP_0), a third degradation phase (c) at T>500°C, hence the respective mass losses of 2.19% and 3.7% correspond to the loss of organic materials such as ethylene molecules, hydrogen, and benzene derivatives, and to the thermal cracking of the heavier non-volatile hydrocarbons of the tyre ash contained in the geopolymeric matrix (Lian et al., 2011). In addition, this distinct phase also indicates an increase in functional groups with the addition of TA to the geopolymer relative to the pristine sample.

3.3. FTIR analysis

Fig. 4 shows the FTIR spectra of the tyre ash (a) and the geopolymer (b), respectively. In Fig. 4a, the vibration band observed between 3853 and 3744 cm^{-1} is attributed to the plane bending vibration of the =C-H bond of the group (Jusli et al., 2014). That bands appearing between 2922 and 2855 cm^{-1} corresponds to the stretching of the -C-H bond of the aliphatic group (Feizi et al., 2020). The weak band at 2243 cm^{-1} is attributed to the C-C stretching vibration of the alkane group. The band

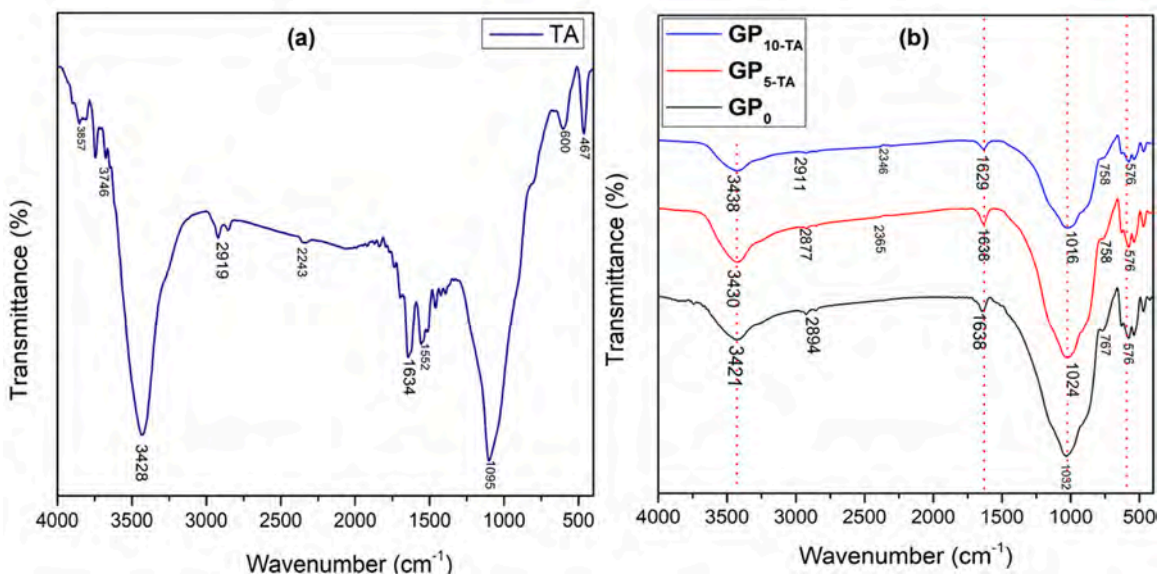

Fig. 4. Spectrum FTIR of TA (a) and geoadsorbent (b).

centered at 1634 cm^{-1} corresponds to the C═O stretching vibration of the carboxyl group and the band around 1557 cm^{-1} is characteristic of the C═C stretching vibration in the aromatic group (Bernardo et al., 2023). The absorption bands at 1095 cm^{-1} and 600 cm^{-1} are characteristic of the C-O stretching of alcohols and aromatic C-H, respectively (Ali et al., 2022). In the spectra of the geopolymers (Fig. 4b), the absorption bands located between 3350 and 3432 cm^{-1} and between 1634 and 1644 cm^{-1} are ascribed to the elongation and deformation vibrations of the O-H bonds of the water molecules adsorbed on the surface or trapped in the pores of the geopolymers, respectively (Dzoujo T et al., 2021). The bands centered between 1027, 1033 cm^{-1} are attributed to the symmetric and asymmetric elongations of the Si-O-Si, and Si-O-Al bonds in the geopolymers and those located between 740 and 769 cm^{-1} are related to the symmetric vibrations of Al-O and Al-OH (Sore et al., 2018). The bands observed around 590 and 468 cm^{-1} correspond, respectively, to symmetrical elongations of Si-O-Si, Al-O-Al, Si-O-Fe and deformations of Si-O-Si, O-Si-O bonds (Tome et al., 2020).

By comparing the spectra of the GP_0 geopolymer with those of the composite geopolymers, it is observed that the addition of tyre ash resulted in the appearance of the C-C vibration bands observed at 2365 and 2346 cm $^{-1}$ within the composites. Consequently, this addition contributes to an increase in the number of chemical functions in the geopolymeric chain. The integration of carbonaceous matter into the geopolymeric network does not always result in a densification of the functional groups, since Tome et al. (2023b) showed that the addition of rice husk ash rather resulted in the shifting of the aluminosilicate bands and an improvement in the geopolymerisation process via the polycondensation/polymerization reaction.

On the other hand, the addition of tyre ash in the geopolymeric network is the origin of the shift of the initial bands reflecting a reorganization of the aluminosilicate phases during geopolymerization. This restructuring with the incorporation of TA could lead to a modification of the textural properties within the structure of the composites and variation in functional group density.

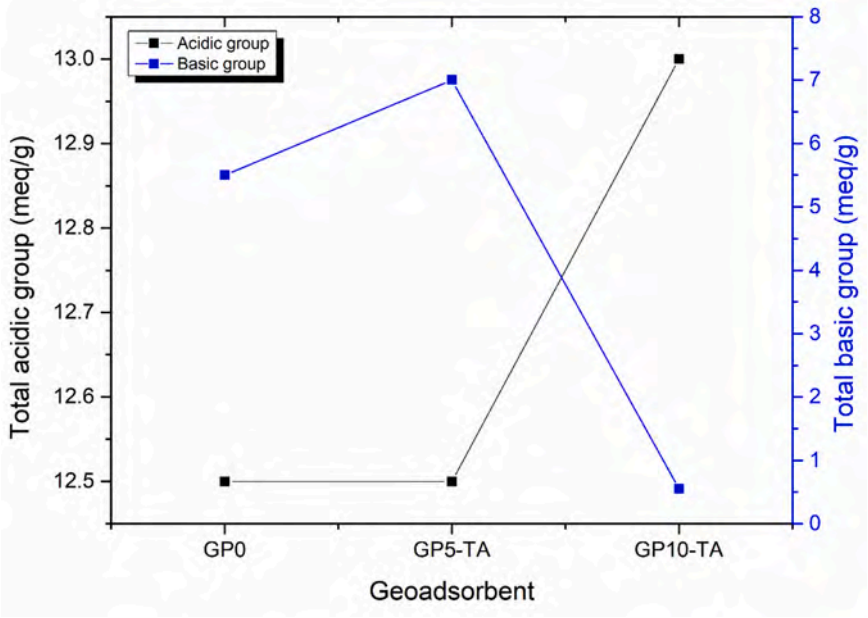

Fig. 5. Content of acid-base functions in geomaterials.

3.4. Total acidic and basic groups analysis

Fig. 5 shows the total number of acidic and basic functional groups present on the surface of geoadsorbents. The geomaterials have more significant content of acidic groups than basic groups due, on the one hand, to the geopolymeric chains made up mainly of silicate and silicate groups from the initial dissolution of the aluminosilicate and, on the other hand, to the carboxylic, hydroxyl, lactonic and carbonyl functions contributed by the TA within the structure of the composites. It is also noted that the $GP_{5\text{-}TA}$ geocomposite also has a higher content of basic functions than $GP_{10\text{-}TA}$, giving the latter an ampholyte character.

3.5. Textural properties analysis

3.5.1. Specific surface area, Iodine and Methylene blue indices

Table 1 highlights the specific surface area values from the BET method and the iodine and methylene blue indices of the geoadsorbents GP_0, $GP_{5\text{-}TA}$ and $GP_{10\text{-}TA}$. It is observed that the addition of 5 and 10% of TA to the geopolymeric matrix led to an increase by ~57 and ~118% in the specific surface area relative to pristine geopolymer, respectively. This also resulted in increase in mesoporosity structure by ~52 and ~40%, respectively. These characteristics are more significant than those reported by Dzoujo Tamaguelon et al. (2022), where incorporating 10% carbonaceous material (biochar) into the geopolymeric matrix only resulted in a 13.2% increase in the specific surface area of the geocomposite obtained. The results show that the effect of equal fraction of an additive on the textural properties depend on the type of material. However, TA incorporation did not have a significant effect on the microporosity.

3.5.2. SEM analysis

Figs. 6 and 7 depict the micrographs of the precursors and geoadsorbents, respectively. Fig. 6 shows that the pozzolan (Pz) has a dense and heterogeneous microstructure in particles corresponding to the different aluminosilate phases present. In contrast, tyre ash (TA) has an amorphous and homogeneous morphology. Moreover, it is observed from the micrograph of the pristine geopolymer (GP_0), a densification of the geopolymeric network due to the polymerization and polycondensation steps that took place during the formation of the geopolymeric chain. Comparing the microstructure of GP_0 with those of the $GP_{5\text{-}TA}$ and $GP_{10\text{-}TA}$ composites (Fig. 7), a notable change in the porosity within the geocomposite structure is observed. This increases with the rate of TA addition to the matrix correlating with the iodine and methylene blue indices reported previously. It is therefore clear that the incorporation of TA into the geopolymeric matrix leads to morphologically distinguishable composites, a modification of the textural properties and changes in the surface chemical functional groups within the resulting geoadsorbent, which could result in remarkable adsorption capabilities.

3.6. Effect of pH of SMX and SDM

Table S2 (supplementary material) associated with Fig. 8 illustrates the significance test for the effect of pH on the adsorption performance of SMX and SDM on the different geopolymers. It was found that the solution pH had no significant effect ($p>0.05$) on the sequestration of SMX on all the geoadsorbents. Consequently, the variation in the quantities of SMX adsorbed (Fig. 8a) on the geopolymers is independent of pH. These observations do not corroborate with the works of Lian et al. (2014) and Shikuku et al. (2020) which reported that SMX retention on biochar was strongly influenced by electrostatic interactions and the ionic form of this adsorbate. Attractive forces, other than coulombic interactions, that are independent of the adsorbent surface charge and ionic form of SMX account for the adsorption process. Furthermore, the wide variability of the pH of effluents imply that the geopolymers present a suitable candidate for SMX sequestration due to their insensitivity to solution pH. In contrast, the retention of SDM on $GP_{5\text{-}TA}$ and $GP_{10\text{-}TA}$ geocomposites was significantly ($p<0.05$) and strongly dependent on pH (Table S1). The favorable binding of SDM observed at pH~6 on the composites (Fig. 8b) is therefore due to the neutral form of sulfadimethoxine (SDM^0), which favors the formation of hydrogen bonding with the negative surface sites of the geocomposites. On the other hand, at $6 < pH < 10$ (Fig. 10b), SDM retention is unfavorable due to the hydrophilic nature of SDM at these pH values, which diminishes the affinity the geocomposites. A strong H-bond [(-) CAHB] assisted by a negative charge between the anionic SDM species above pH 6 and the -OH groups of the aluminosilicate material is postulated as a possible operational mechanism (Shikuku et al., 2018). Similar interpretations were mentioned by Xie et al. (2021) during studies on the detection of sulfonamides and quinolones in water. Since maximum adsorption of SDM is observed at circumneutral pH values, and the uptake of SMX is unaffected by pH, the geopolymer composites are therefore suitable candidates for the sequestration of these sulfonamides at near natural pH of surface waters.

Table 1
Specific area, Iodine and Methylene blue indices of adsorbents.

Adsorbents	GP_0	$GP_{5\text{-}TA}$	$GP_{10\text{-}TA}$
S_{BET} ($m^2.g^{-1}$)	13.62	21.48	29.70
Iodine index ($mg.g^{-1}$)	317.25	482.22	444.15
Methylene blue index ($mg.g^{-1}$)	20.76	21.81	24.74

3.7. Kinetic study of SMX and SDM

Fig. 9 shows the evolution of the quantities of SMX (Fig. 9a) and SDM (Fig. 9b) adsorbed on the geoadsorbents GP_0, $G_{P5\text{-}TA}$ and $GP_{10\text{-}TA}$. A rapid fixation of the adsorbates is observed at the very beginning of the process followed by an equilibrium state after 60 and 150 min for SMX and SDM, respectively. The rapid adsorption observed is due to the availability of vacant active sites while the steady state corresponds to a progressive saturation of energetically favorable sites. Furthermore, it should be noted that the $GP_{10\text{-}TA}$ geopolymer composite exhibits a higher SMX and SDM removal rate (39.56 and 52.22%, respectively) than the GP_0 and $GP_{5\text{-}TA}$ adsorbents due to its more significant textural properties. To understand the mechanisms governing the adsorption kinetics of these sulfonamides on the surface of geopolymers, the experimental data were modeled with the pseudo first-order (Ho and Mckay, 1998) and pseudo second-order (Ho, 2006) kinetic models expressed by Eqs. 4 and 5, respectively.

$$\text{Pseudo First Order}: q_t = q_e\left(1 - e^{-k_1 t}\right) \tag{4}$$

Where q_t (mg/g) is the adsorbed amount at time t (min), k_1 (min^{-1}) is the pseudo-first-order rate constant and q_e is the amount adsorbed at equilibrium.

$$\text{Pseudo Second Order}: q_t = \frac{k_2 q_e^2 t}{1 + k_2 q_e t} \tag{5}$$

$$K_2 q_e = \frac{1}{t_{1/2}} \text{ and } S_{rate} = k_2 q_e^2 \tag{6}$$

Where: K_2 ($g.mg^{-1}.min^{-1}$) is the pseudo-second-order rate constant, $t_{1/2}$ is the adsorption half-life and S_{rate} (mg/g.min) is the initial adsorption rate.

From Table 2, the pseudo-second order (PSO) kinetic model best fits the experimental data on all adsorbents based on closeness of the coefficients of determination R^2 values to unity and the model-predicted data also converging closer to the experimentally obtained data (Figs. S1 and S2). In addition, the PSO model indicates that chemisorption is the rate-determining step controlling the binding of SMX and SDM to the geopolymer surface. In general, adsorption of SDM exhibited

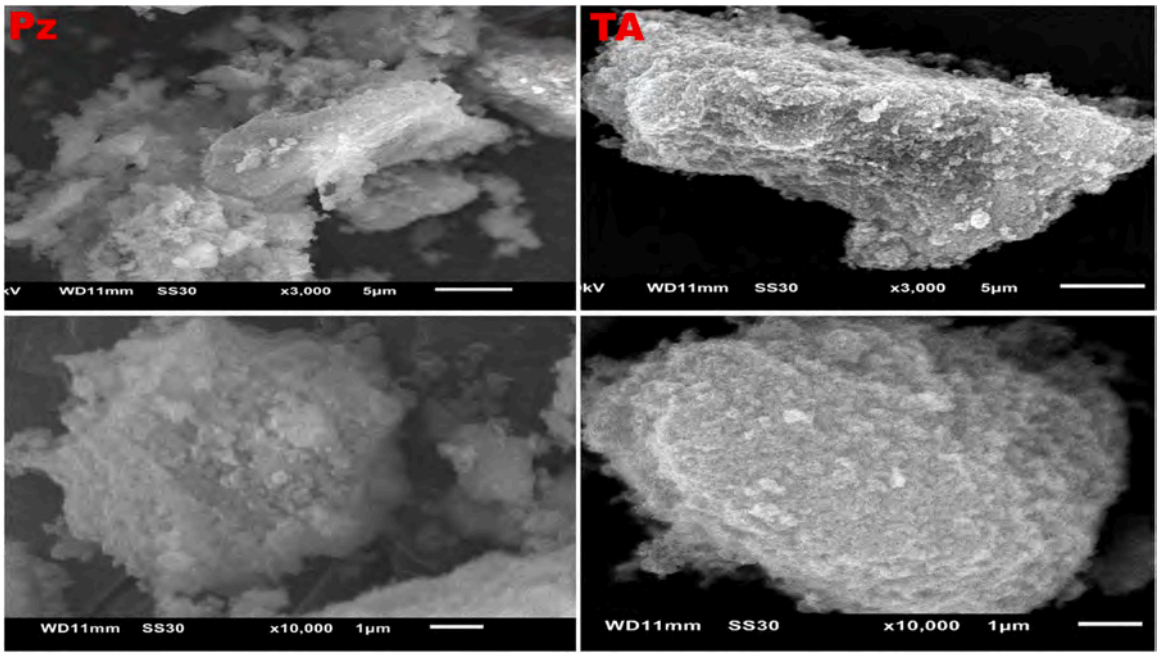

Fig. 6. Microstructure of the raw materials.

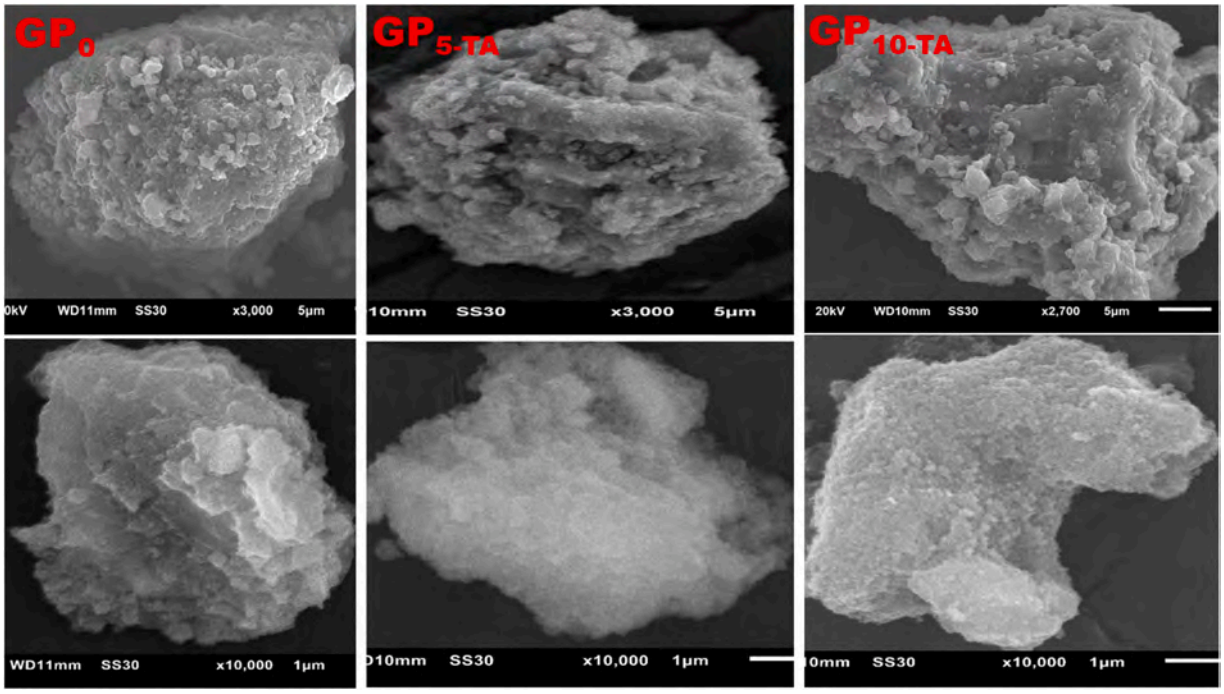

Fig. 7. Microstructure of GP_0, $GP_{5\text{-}TA}$ and $GP_{10\text{-}TA}$ geoadsorbents.

shorter half-life than SMX indicating preferential adsorption of SDM. The rate constant (k_2) did not follow any obvious pattern signifying an interplay between textural properties, functional group density and distribution, and molecular properties.

3.8. Isothermal study of SMX and SDM

To define the mechanisms by which SMX and SDM sequestration react on composites in the aqueous and saline phases, the experimental data were fitted to two- and three-parameter isotherms, respectively.

3.8.1. two-parameter isotherm modelling

3.8.1.1. Langmuir isotherm. Langmuir model generally defines monolayer adsorption phenomena on energetically equivalent binding sites (Langmuir, 1916). The expression and separation constant associated with this isotherm are given respectively by Eqs. (6) and (8)

$$q_e = \frac{q_{\max} K_L C_e}{1 + K_L C_e} \tag{7}$$

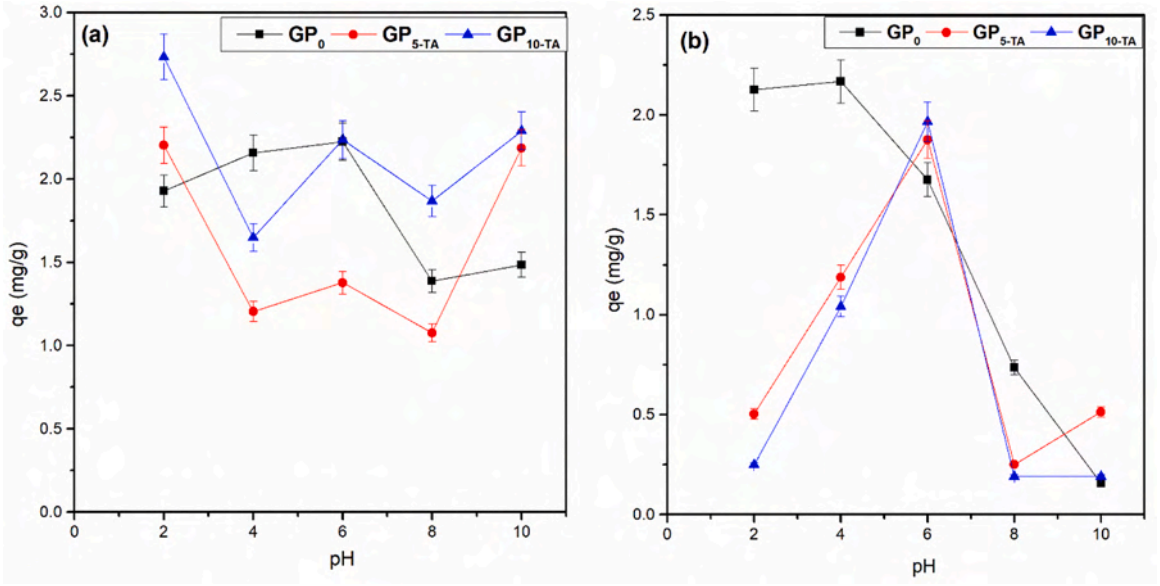

Fig. 8. Influence of pH on the adsorption of (a) SMX and (b) SDM onto GP_0, $GP_{5\text{-}TA}$ and $GP_{10\text{-}TA}$ geomaterials.

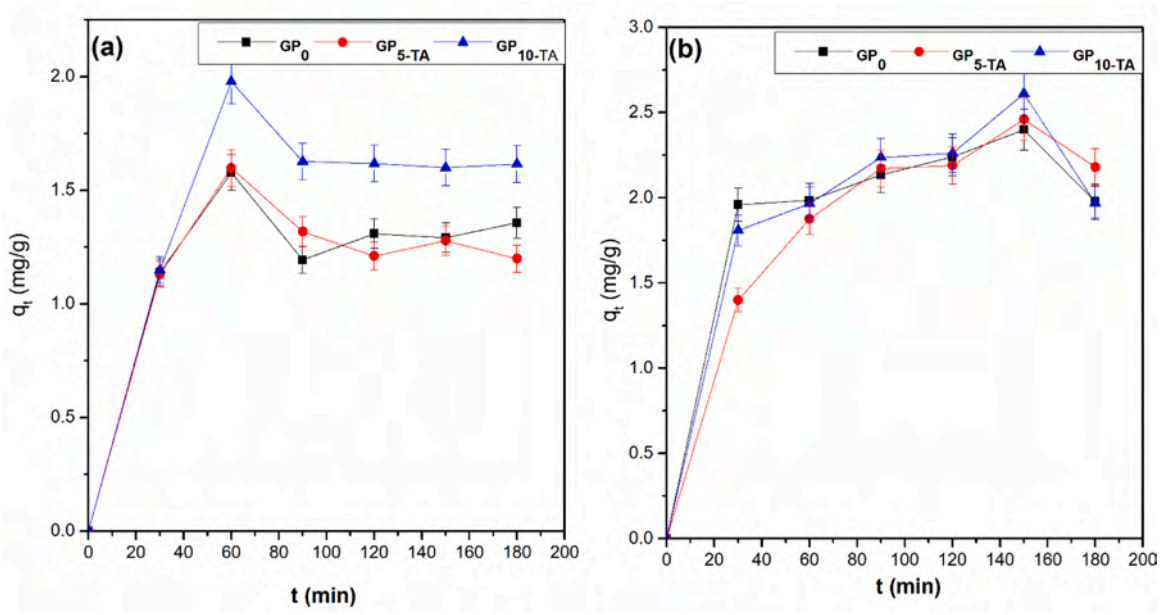

Fig. 9. Influence of SMX (a) and SDM (b) contact time on the adsorption capacities of GP_0, $GP_{5\text{-}TA}$ and $GP_{10\text{-}TA}$ geomaterials.

$$R_L = \frac{1}{1 + K_L C_0} \tag{8}$$

Where qe is the equilibrium adsorbed quantity (mg/g), q_{max} is maximum adsorbable quantity (mg/g), K_L is the Langmuir constant (L/g) and C_e is the equilibrium liquid phase concentration (mg/L) and C_o is the initial concentration (mg/L).

The apparent equilibrium constant (Ka), a product of q_{max} and K_L, is an index of geopolymers' affinity to the adsorbate molecules. The higher the Ka value, the higher the affinity (Luttah et al., 2023). The separation constant, R_L, denotes the favorability of the adsorption process. Based on the low coefficients of determination (R^2) and high associated error functions (Table 4), the Langmuir model is unable to explain the mechanisms of SMX adsorption in both aqueous and saline media on the different adsorbents. On the other hand, this isotherm (Table 5) could appreciably predict the fixation of SDM on GP_0 and $GP_{10\text{-}TA}$ geoadsorbents in the aqueous phase.

3.8.1.2. Freundlich model. This empirical model describes multilayer adsorption mechanisms on exponentially heterogeneous sites (Freundlich, 1906).The expression for the Freundlich isotherm is given by Eq. 9.

$$q_e = K_F C_e^{1/n} \tag{9}$$

Where K_F ($L.g^{-1}$) and n are, the Freundlich constant and coefficient related the favorability of the adsorption process, respectively.

The relatively high coefficients of determination (R^2) values (Table 3) show that the Freundlich model fits the equilibrium data for the retention of SMX onto GP_0 and $GP_{5\text{-}TA}$ geopolymers in both aqueous and saline environments. However, this isotherm (Table 4) was insufficient to explain the mechanism of SDM adsorption in a saline environment within these adsorbents. The values of $1/n > 1$ indicate weak adsorbent-adsorbate interactions corresponding to a physisorption

Table 2
Parameters obtained from SMX and SDM kinetic models.

Models	Parameters	GP_0		$GP_{5\text{-}TA}$		$GP_{10\text{-}TA}$	
Pseudo-first order		SMX	SDM	SMX	SDM	SMX	SDM
	K_1 (min^{-1})	2.00	1	2.52	2.52	2.00	1
	$q_{e\ (cal)}$ (mg.g^{-1})	1.31	2.12	1.29	2.05	1.59	2.14
	$q_{e\ (exp)}$ (mg.g^{-1})	1.58	2.40	1.60	2.46	1.98	2.61
	R^2	0.93	0.96	0.91	0.84	0.86	0.90
Pseudo-second order	K_2 (g.mg^{-1}.min^{-1})	0.21	0.09	0.57	0.01	0.06	0.04
	$q_{e\ (cal)}$ (mg.g^{-1})	1.37	2.26	1.31	2.70	1.80	2.43
	$q_{e\ (exp)}$ (mg.g^{-1})	1.58	2.40	1.60	2.46	1.98	2.61
	$t_{1/2}$ (min)	0.15	0.04	0.44	0.005	0.03	0.02
	S_{rate}	0.39	0.45	0.98	0.10	0.19	0.29
	R^2	0.93	0.97	0.91	0.98	0.90	0.94

mechanism. Similar results were reported by Shikuku and Jemutai-kimosop (2020) during SMX removal onto biochar derived from sugarcane bagasse.

3.8.1.3. Flory Huggins model. The Flory Huggins model elucidates the feasibility and spontaneity of the adsorbate fixation mechanisms on the adsorbent surface (Flory, 1953). The mathematical expression of this isotherm is given by Eq. (10).

$$\frac{\theta}{c_0} = K_{FH}(1-\theta)^{n_{FH}} \text{With} \theta = 1 - \frac{c_e}{c_0} \quad (10)$$

Where K_{FH} ($L.g^{-1}$) is the equilibrium constant for determining the Gibbs free energy and φ_W (1000 g/L) is the density of water (Eq. 11)

$$\Delta G = -RT \ln K_{FH}\phi_W \quad (11)$$

Unlike the Langmuir and Freundlich isotherms, the Flory Huggens model is the most appropriate for describing the mechanisms of SMX and SDM abatement on the $GP_{10\text{-}TA}$ geopolymer composite in both environments based on R^2 >0.90 and relatively low Chi-square (Table 4 and Table 5). The negative and ΔG <20 $kJ.mol^{-1}$ values indicate that SMX and SDM binding on $GP_{10\text{-}TA}$ is thermodynamically spontaneous and that physical-type interactions predominate among the interactions likely to take place (Fig. 10).

Despite the R^2 >0.90 of the two-parameter isotherms, the SMX retention mechanism in the saline phase is governed mainly by Freundlich for GP_0 and $GP_{5\text{-}TA}$ and Flory-Huggens for $GP_{10\text{-}TA}$. Unlike the GP_0 and $GP_{5\text{-}TA}$ geoadsorbents, only the Flory-Huggens model describes the process controlling the lowering of SDM on $GP_{10\text{-}TA}$ in this environment. These are implicit evidences for interplay between adsorbent characteristics, process conditions and adsorbate properties.

3.8.2. Three-parameter isotherm modelling

3.8.2.1. Sips isotherm. The Sips isotherm provides a satisfactory prediction of adsorption mechanisms on heterogeneous surfaces, assuming that the adsorbates occupy more binding sites and excluding adsorbate-adsorbate interactions (Sips, 2004). The expression of this model is given by Eq. 12.

Table 3
SMX data resulting from 2-parameter isothermal models studied in aqueous and saline environments.

Isotherms	Parameters	GP_0	$GP_{0\ (S)}$	$GP_{5\text{-}TA}$	$GP_{5\text{-}TA\ (S)}$	$GP_{10\text{-}TA}$	$GP_{10\text{-}TA\ (S)}$
Langmuir	q_{max} (mg.g^{-1})	0.70	2.69	0.98	1.36	1.06	4.00
	K_L (L.mg^{-1})	0.84	0.20	0.80	0.90	0.91	0.15
	Ka (L.g^{-1})	0.59	0.54	0.78	1.22	0.97	0.60
	RL	0.19	0.51	0.20	0.18	0.18	0.57
	χ^2	6.42	2.12	20.08	3.68	2.66	1.24
	R^2	0.77	0.81	0.62	0.76	0.63	0.89
Freundlich	K_F (L.mg^{-1})	0.01	0.16	0.10	0.10	0.31	0.47
	1/n	4.30	1.98	2.32	3.18	1.61	1.00
	χ^2	0.01	0.12	1.56	0.10	1.10	1.08
	R^2	**0.99**	**0.98**	**0.91**	**0.95**	0.72	0.77
Flory Huggens	K_{FH}	0.24	0.30	0.28	0.38	0.36	0.36
	ΔG ($kJ.mol^{-1}$)	-13.59	-14.13	-13.97	-14.82	-14.58	-14.58
	n_{FH}	0	0	0	0	0	0
	χ^2	4.29	1.00	8.97	1.51	1.37	0.63
	R^2	0.77	0.91	0.83	0.87	**0.92**	**0.93**

(s): saline environment.

Table 4
SDM data resulting from 2-parameter isothermal models studied in aqueous and saline environments.

Isotherms	Parameters	GP_0	$GP_{0\ (S)}$	$GP_{5\text{-}TA}$	$GP_{5\text{-}TA\ (S)}$	$GP_{10\text{-}TA}$	$GP_{10\text{-}TA\ (S)}$
Langmuir	Q_{max} (mg.g^{-1})	3.70	426.23	1.48	1.66	3.32	1.79
	K_L (L/mg)	0.19	0.001	0.45	0.38	0.24	0.93
	Ka (L/g)	0.70	0.43	0.67	0.63	0.80	1.67
	R_L	0.52	0.99	0.31	0.34	0.45	0.18
	χ^2	0.48	0.42	1.73	1.57	0.40	1.71
	R^2	0.92	0.80	0.86	0.64	0.93	0.65
Freundlich	K_F (L.mg^{-1})	0.30	0.36	0.08	0.27	0.54	0.59
	1/n	1.68	0.90	2.66	1.30	1.09	1.27
	χ^2	0.01	0.44	0.09	0.83	0.34	0.96
	R^2	**0.99**	0.75	**0.95**	0.77	0.79	0.69
Flory Huggens	K_{FH}	0.36	0.25	0.31	0.27	0.38	0.43
	ΔG ($kJ.mol^{-1}$)	-14.59	-13.66	-14.21	-13.89	-14.69	-15.04
	n_{FH}	0	0	0	0	0	0
	χ^2	0.19	0.21	0.88	0.68	0.11	0.45
	R^2	0.96	0.85	0.87	0.86	**0.98**	**0.95**

Table 5
SMX data resulting from 3-parameter isothermal models studied in aqueous and saline environments.

Isotherms	Parameters	GP_0	$GP_{0\ (S)}$	$GP_{5\text{-}TA}$	$GP_{5\text{-}TA\ (S)}$	$GP_{10\text{-}TA}$	$GP_{10\text{-}TA\ (S)}$
Sips	q_{ms} (mg.g^{-1})	5.77	4.66	1.42	46.69	1.74	1.50
	a_s	0.0006	0.03	1.35E-05	0.002	0.0003	0.16
	B_S	5.22	2.55	14.67	3.24	13.18	4.68
	$\chi 2$	0.03	0.07	0.09	0.10	**0.17**	0.07
	R^2	**0.99**	**0.98**	**0.96**	**0.95**	**0.94**	0.94
Koble Corrigan	A	0.008	0.12	0.0003	0.01	4.49E-06	0.32
	B	0	0.03	0.0002	0	2.44E-06	0.18
	n_k	4.30	2.55	10.76	3.19	20.53	3.16
	$\chi 2$	0.008	0.07	0.17	0.10	0.34	**0.09**
	R^2	**0.99**	**0.98**	0.96	**0.95**	0.93	**0.97**
Toth	q_{mT}	1.55	1.72	1.65	2.00	2.01	1.94
	z	56.32	65.01	62.26	78.91	1.03	70.55
	a_T	7.95E+39	7.94E+39	7.94E+39	7.92E+39	7.93E+39	7.92+39
	$\chi 2$	6.68	1.95	16.03	3.68	3.10	1.00
	R^2	0.60	0.81	0.68	0.65	0.75	0.91

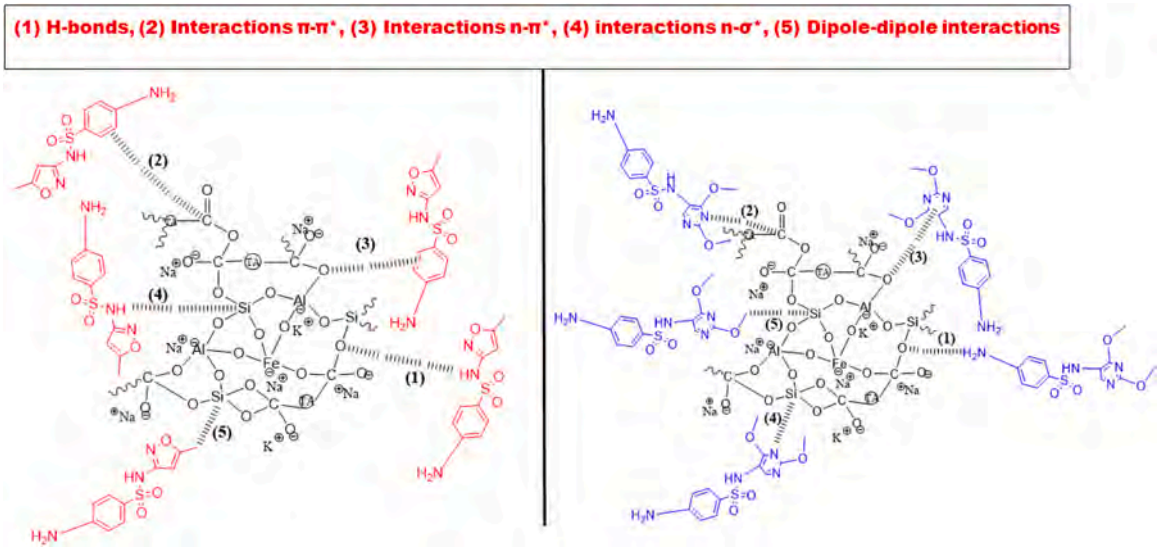

Fig. 10. Possible interactions of SMX and SDM fixation on the geocomposite.

$$q_e = \frac{q_{ms} a_s C_e^{B_s}}{1 + a_s C_e^{B_s}} \quad (12)$$

Where q_{ms} (mg/g): is the sips maximum adsorption capacity, a_s (L/mg): is the sips equilibrium constant and B_s is the heterogeneity index.

$R^2 > 0.90$ and the relatively low χ^2 values (Table 5 and Table 6) attest to the adaptability of the Sips model in correlating equilibrium data for SMX and SDM adsorption for all the geopolymers in both aqueous and saline environments. The adsorption capacities were therefore compared based on the Sips model. The parameter Bs > 1 reflect highly heterogeneous adsorbent-adsorbate systems corroborating with the Freundlich isotherm. The theoretical SMX sequestration capacities (Table 5) decreased in the saline environment from 5.77 to 4.66 mg/g for GP_0 and from 1.74 to 1.50 mg/g for $GP_{10\text{-}TA}$. This is due to the very

Table 6
SDM data resulting from 3-parameter isothermal models studied in aqueous and saline environments.

Isotherms	Parameters	GP_0	$GP_{0\ (S)}$	$GP_{5\text{-}TA}$	$GP_{5\text{-}TA\ (S)}$	$GP_{10\text{-}TA}$	$GP_{10\text{-}TA\ (S)}$
Sips	Q_{max} (mg.g^{-1})	28.34	1.08	107.69	1.21	1.85	2.08
	a_s	0.01	0.0003	0.001	3.66E-06	0.17	0.0001
	B_S	1.75	14.65	2.68	19.62	3.99	17.31
	$\chi 2$	0.01	0.14	0.10	0.28	0.19	0.29
	R^2	**0.99**	**0.97**	0.95	**0.93**	0.88	0.96
Koble Corrigan	A	0.30	0.001	0.08	0.0003	1.09306E-05	0.002
	B	0	0.001	0	0.0002	6.75E-06	0.001
	n_k	1.68	13.03	2.66	12.93	37.16	13.56
	$\chi 2$	0.01	0.14	0.09	0.41	0.55	0.28
	R^2	**0.99**	**0.97**	**0.96**	0.89	0.76	**0.98**
Toth	q_{mT}	2.08	1.10	1.75	1.84	2.00	2.21
	z	71.34	22.04	36.96	60.91	117.55	171.96
	a_T	3.82E+40	2.82 E+10	2.45E+22	6.14E+42	3.12E+61	3.11E+81
	$\chi 2$	0.45	0.43	1.71	1.22	0.27	1.29
	R^2	0.89	0.81	0.73	0.74	**0.95**	0.76

pronounced competition between the Cl^- ions in solution and the anionic SMX for the same active sites and cationic SMX with Na^+ adsorbed through ion exchange (Wang et al., 2022). In contrast, the increase in model-predicted SMX adsorption capacity on the $GP_{5\text{-}TA}$ geopolymer composite from 1.42 to 46.69 mg/g is attributed to the more significant density of basic functional groups within this geopolymer which counteract the repulsive and competitive interactions. This can be partly deduced from the apparent equilibrium constant, Ka. Similar, but exacerbated, adsorption in saline environment was observed for SDM. Noteworthy, the model-predicted quantities of SDM adsorbed on the GP_0 and $GP_{5\text{-}TA}$ geomaterials (Table 6) were substantially higher (28.34 and 107.69 mg/g, respectively) in the aqueous phase implying the SDM structure offers more interaction sites with the surface functions of these adsorbents. These interpretations are consistent with the findings of Wang et al. (2022) that the preparation of tetracycline solutions in saline water had an influence on the adsorption performance of oleic acid-modified metakaolin-based geopolymers. However, these results reveal that the adsorption capacities of geopolymer composites are not controlled solely by the specific surface area (SSA) but rather by the synergy between textural properties, competing ions and the density of surface functional groups.

3.8.2.2. Koble-Corrigan isotherm. The Koble-Corrigan model combining the Langmuir and Freundlich isotherms is used to predict the adsorption mechanisms for heterogeneous systems (Koble and Corrigan, 1952). Eq. 13 is the expression for the Koble isotherm.

$$q_e = \frac{AC_e^{n_k}}{1 + BC_e^{n_k}} \tag{13}$$

Where A, B and n_k are Koble-Corrigan isotherm constants.

Given the values of nk > 1 and the coefficients of determination close to unity (Table 6 and Table 7), the Koble model is in line with the equilibrium data as from the Sips isotherm in describing the mechanisms linked to the respective sequestrations of SMX on the GP_0, $GP_{5\text{-}TA}$ and $GP_{10\text{-}TA}$ geoadsorbents and of SDM on GP_0 and $GP_{10\text{-}TA}$ in the saline phase. Furthermore, in accordance with the parameters n_F and Bs (greater than unity) derived from the Freundlich and Sips isotherms respectively, the values of $n_k > 1$ also attest that the adsorption of SMX and SDM takes place in multilayers on the heterogeneous surface sites of these geoadsorbents.

3.8.2.3. Toth isotherm. The Toth isotherm is an empirical model used to describe heterogeneous adsorption systems for low and high concentrations of adsorbates (Toth, 1971). Eq. 14 is the expression of this model.

$$q_e = \frac{q_{mT}c_e}{\left(a_T + c_e^z\right)^{1/z}} \tag{14}$$

Where q_{mT}, a_T and z are Toth maximum adsorption capacity, Toth equilibrium constant and Toth model exponent respectively.

In contrast to the Sips and Koble-Corrigan isotherms, the Toth model is applicable to equilibrium data to describe the mechanism controlling the binding of SDM to $GP_{10\text{-}TA}$ in the aqueous phase despite R^2 converging towards unity (Table 6). In addition, the deviation of the z parameter from unity indicates a very heterogeneous $GP_{10\text{-}TA}$-SDM system and thus corroborates the deductions of the Sips and Koble models.

The 3-parameter isotherms show sufficient variation in the SMX and SDM retention mechanisms at the surface of the geoadsorbents under the effect of Na^+ and Cl^- ions added to the medium. Furthermore, it is noted that the SMX adsorption isotherms for the $GP_{5\text{-}TA}$ and $GP_{10\text{-}TA}$ geosorbents in saline solution (Figs. S3 and S5, supplementary material) exhibit an H-type representation indicating a high affinity of the solute for the adsorbent in this environment. In contrast, the SDM binding isotherms show a sigmoidal shape (Figs. S4 and S6, supplementary material) revealing that at least two mechanisms govern SDM retention in the saline phase.

3.9. Mechanism and comparison with other adsorbents

Comparison of the removal capacities of the geopolymers in this study with other adsorbents in the literature (Table 7) reveals that the $GP_{5\text{-}TA}$ geopolymer composite exhibits a high performance for the sequestration of SDM in aqueous media, relative to other sorbents. Table 7 also reveals the lack of adsorption data for sulfonamides in saline solution.

Fig. 11 highlights the mechanisms responsible for the adsorption dynamics of SMX and SDM on the $GP_{5\text{-}TA}$ geopolymer composite in aqueous and saline environments. The high adsorption capacity of SDM compared with SMX on $GP_{5\text{-}TA}$ in the aqueous phase is explained by the high reactivity of ring (b) of SDM, since it has two free reactive doublets on the nitrogen, so the charges on these are strengthened by the donor groups through the mesomeric and inductive -OCH_3 effect, thus promoting n-σ* and n-π* interactions between this portion of SDM and the structure of the composite. On the other hand, the non-bonding doublet on ring (a) of SMX is less reactive due to the inductive donor group -CH_3, which is very far away from this doublet, giving it a low electronic contribution that hinders interactions with this site.

Furthermore, the good ability of the $GP_{5\text{-}TA}$ geocomposite to bind

Table 7
Comparative data on adsorption performance in SMX and SDM between the geoadsorbents studied and those from previous work.

Adsorbent	SMX		SDM		References
	Aqueous phase adsorption capacity (mg/g)	salt phase adsorption capacity (mg/g)	Aqueous phase adsorption capacity (mg/g)	salt phase adsorption capacity (mg/g)	
Biochar (CBG)	128	-	-	-	(Shikuku and Jemutai-kimosop, 2020)
Clay	-	-	1.39	-	(Shikuku et al., 2017)
core-shell activated carbon (CSAC)	6.3	-	-	-	(Ndagijimana et al., 2019)
hydrous ferric oxides (HFO)	-	-	1.30		(Zhu et al., 2018)
ordered mesoporous carbon	334	-	-	-	(Sarker et al. 2023)
Iron modified clay	-	-	1.78	-	(Shikuku et al., 2018)
Reclaimed activated carbon	16.15	-	-	-	(Liu et al. 2019)
$FeCl_3$-magnetized biochar	454.5	-	-	-	(Sun et al., 2022)
GP_0	5.77	4.66	28.34	1.08	This study
$GP_{5\text{-}TA}$	1.42	**46.69**	**107.69**	1.21	This study
$GP_{10\text{-}TA}$	1.74	1.50	1.87	2.08	This study

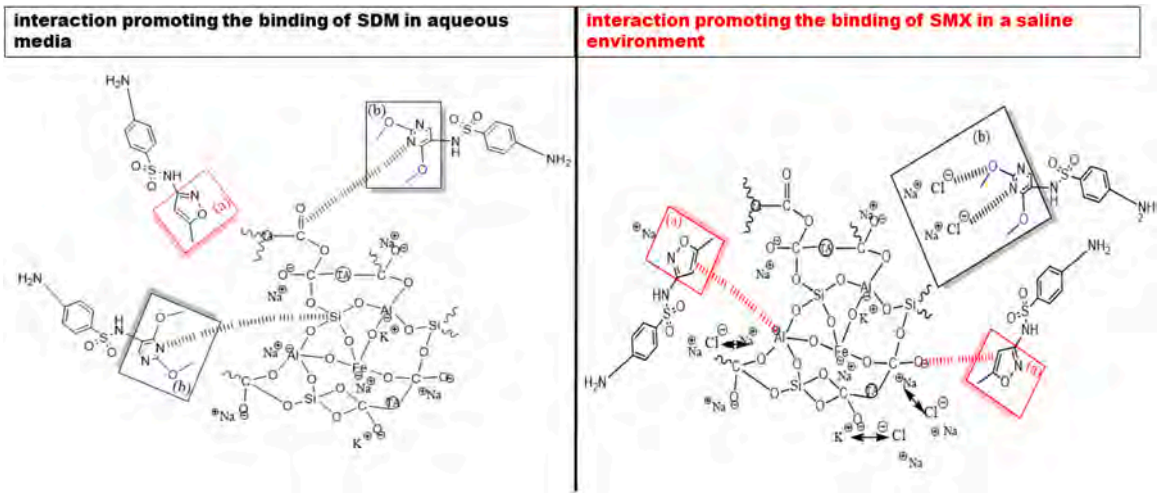

Fig. 11. Demonstration of the process promoting the fixation of SDM and SMX in aqueous and saline environment.

SMX in a saline environment is due to the fact that the Cl- ions provided by the NaCl associate electrostatically with all the alkaline counter ions (Na^+ and K^+) present on the surface of the composite, thereby freeing the oxygen, aluminium and iron reaction sites. The released reaction sites can therefore create n-π* interactions with the SMX ring (a). In addition, the highly reactive ring (b) of SDM will interact with the Cl^- ions, resulting in van der Waals bonds and consequently increasing the solubility of SDM in this environment and hindering its bonding to the $GP_{5\text{-}TA}$ composite. Similar interactions have been reported for the adsorption of tetracycline onto geopolymer adsorbent (Jin et al., 2024).

4. Conclusion

The present work evaluated the performance of geopolymers derived from pozzolan (a natural resource) with various fractions of tyre ash (TA) (an industrial waste) for the abatement of sulfamethoxazole (SMX) and sulfadimethoxine (SDM) under various environmental conditions. Relative to pristine geopolymer (GP_0), the incorporation of 5 and 10% TA increased the specific surface area (SSA) from 13.62 to 21.48 ($GP_{5\text{-}TA}$) and 29.70 m^2/g ($GP_{10\text{-}TA}$), respectively. The equilibrium data was best described by the Sips isotherm model. Salinity significantly diminished the adsorption of both SMX and SDM. In a non-saline aqueous medium, the geopolymers exhibited higher adsorption capacity for SDM relative to SMX. In contrast, in saline medium, SMX uptake was higher. Adsorption of SMX was unaffected by pH whilst SDM removal was significantly pH-dependent. The $GP_{5\text{-}TA}$ geopolymer composite exhibited the highest adsorption capacity for SMX in a saline environment (46.69 $mg.g^{-1}$) and for SDM in an aqueous environment (107.69 $mg.g^{-1}$). The adsorption kinetics of SMX and SDM are controlled by the pseudo-second-order law. The magnitude of free energy (ΔG~-13–15 $kJ.mol^{-1}$) indicates that the adsorption processes are spontaneous and physical. The results provide fresh evidence on the sequestration of sulfonamides using geopolymers and the driving factors and open new challenges of development of superior adsorbents for sulfonamides removal, especially in saline waters.

Ethical approval and consent to participate

Not applicable.

Funding

This work was supported by AGNES (African-German Network of Excellence in Science).

CRediT authorship contribution statement

David Daniel Joh Dina: Writing – review & editing. **Marie Annie Etoh:** Writing – review & editing. **Hermann Dzoujo Tamaguelon:** Investigation, Methodology, Writing – original draft, Funding acquisition. **Victor Shikuku:** Data curation, Supervision, Writing – review & editing. **Fidele Gallo Titini:** Data curation, Writing – review & editing. **Sylvain Tome:** Conceptualization, Data curation, Writing – review & editing. **Till Strothmann:** Resources, Writing – review & editing. **Pamela Ondiek:** Investigation. **Christoph Janiak:** Resources, Writing – review & editing. **Zachary Getenga:** Funding acquisition, Supervision, Writing – review & editing.

Declaration of Competing Interest

The authors declare that they have no known competing financial interests or personal relationships that could have appeared to influence the work reported in this paper

Acknowledgement

Hermann Dzoujo Tamaguelon thanks the African-German Network of Excellence in Science (AGNES) for granting a Mobility Grant in 2022 to carry out the work presented in this article; the Grant is generously sponsored by German Federal Ministry of Education and Research and supported by the Alexander von Humboldt Foundation. The authors are grateful to the Kenya Standard Bureau (KEBS), the Analytical Chemistry Laboratory of Machakos University in Kenya and the Institute of Inorganic and Structural Chemistry in Düsseldorf, Germany, for providing all the facilities needed to carry out the various analyses and characterizations.

Consent for publication

Not applicable.

Appendix A. Supporting information

Supplementary data associated with this article can be found in the online version at doi:10.1016/j.cherd.2024.05.009.

References

Acosta, R., Fierro, V., Martinez de Yuso, A., Nabarlatz, D., Celzard, A., 2016. Tetracycline adsorption onto activated carbons produced by KOH activation of tyre pyrolysis

char. Chemosphere 149, 168–176. https://doi.org/10.1016/j.chemosphere.2016.01.093.
Ali, U.F., Hussin, F., Gopinath, S.C.B., Aroua, M.K., Khamidun, M.H., Jusoh, N., Ibrahim, N., Faraheen, S., Ahmad, K., 2022. Advancement in recycling waste tire activated carbon to potential adsorbents. Environ. Eng. Res. 27, 0–1.
Bernardo, M., Lapa, N., Pinto, F., Nogueira, M., Matos, I., Ventura, M., 2023. Valorisation of spent tire rubber as carbon adsorbents for Pb (II) and W (VI) in the framework of a Circular Economy. Environ. Sci. Pollut. Res. https://doi.org/10.1007/s11356-023-27689-5.
Chebii, F., K'oreje, K., Okoth, M., Lutta, S., Masime, P., Demeestere, K., 2024. Occurrence and environmental risks of contaminants of emerging concern across the River Athi Basin, Kenya, in dry and wet seasons. Sci. Total Environ. 914, 169696 https://doi.org/10.1016/j.scitotenv.2023.169696.
Chen, J., Xie, S., 2018. Overview of sulfonamide biodegradation and the relevant pathways and microorganisms. Sci. Total Environ. 640–641, 1465–1477. https://doi.org/10.1016/j.scitotenv.2018.06.016.
Dzoujo T, H., Tome, S., Shikuku, V.O., Tchuigwa, J.B., Spieß, A., Janiak, C., Etoh, M.A., Daniel, D., Dina, J., Daniel, D., Dina, J., 2021. Enhanced performance of hydrogen peroxide modified pozzolan-based geopolymer for abatement of methylene blue from aqueous medium. Silicon 14, 5191–5206. https://doi.org/10.1007/s12633-021-01264-4.
Dzoujo Tamaguelon, H., Shikuku, V.O., Tome, S., Akiri, S., Kengne, N.M., Abdpour, S., Janiak, C., Annie, M., Dina, D., 2022. Synthesis of pozzolan and sugarcane bagasse derived geopolymer-biochar composites for methylene blue sequestration from aqueous medium. J. Environ. Manag. 318, 115533 https://doi.org/10.1016/j.jenvman.2022.115533.
Elgarahy, A.M., Maged, A., Eloffy, M., Zahran, M., Kharbish, S., Elwakeel, K.Z., Bhatnagar, A., 2023. Geopolymers as sustainable eco-friendly materials: Classification, synthesis routes, and applications in wastewater treatment. Sep. Purif. Technol. 324, 124631 https://doi.org/10.1016/j.seppur.2023.124631.
Feizi, F., Reguyal, F., Antoniou, N., Zabaniotou, A., Sarmah, A.K., 2020. Environmental remediation in circular economy: end of life tyre magnetic pyrochars for adsorptive removal of pharmaceuticals from aqueous solution. Sci. Total Environ. 739, 139855 https://doi.org/10.1016/j.scitotenv.2020.139855.
Flory, P.J., 1953. Principles of Polymer Chemistry. Cornell University Press, New York.
Freundlich, H., 1906. Über die adsorption in lösungen. Z. Phys. Chem. 57, 385–470. https://doi.org/10.1515/zpch-1907-5723.
Guo, X., Wang, J., 2019. Sorption of antibiotics onto aged microplastics in freshwater and seawater. Mar. Pollut. Bull. 149, 110511 https://doi.org/10.1016/j.marpolbul.2019.110511.
Ho, Y., 2006. Review of second-order models for adsorption systems. J. Hazard. Mater. 136, 681–689. https://doi.org/10.1016/j.jhazmat.2005.12.043.
Ho, Y.S., Mckay, G., 1998. Sorption of dye from aqueous solution by peat. Chem. Eng. J. 70, 115–124.
Jacques, M.B., Guy, N.P., Jules, M.L., Harlette, Z.P., Maffeu, E.J., Said, M., Doungmo, G., Shikuku, V.O., Tchieta, G., Kamdem, F., 2023. Removal of crystal violet by TiO2 loaded alkali-activated carbon hybrid material from Raphia farinifera fruit kernels: surface chemistry, parameters and mechanisms. Biomass-.-. Conv. Bioref. https://doi.org/10.1007/s13399-023-04988-y.
Jemutai-kimosop, S., Okello, V.A., Shikuku, V.O., Orata, F., 2022. Synthesis of mesoporous akaganeite functionalized maize cob biochar for adsorptive abatement of carbamazepine: kinetics, isotherms, and thermodynamics Synthesis of mesoporous akaganeite functionalized maize cob biochar for adsorptive abatement of carba. Clean. Mater. 5, 100104 https://doi.org/10.1016/j.clema.2022.100104.
Jemutai-Kimosop, S., Orata, F., Shikuku, V.O., Okello, V.A., Getenga, Z.M., 2019. Insights on adsorption of carbamazepine onto iron oxide modified diatomaceous earth: Kinetics, isotherms, thermodynamics, and mechanisms. Environ. Res. 180, 108898 https://doi.org/10.1016/j.envres.2019.108898.
Jin, H., Qiu, C., Li, Y., Liu, J., Zhang, D., Chen, Q., Lu, X., Li, C., Wang, Q., 2024. Insight into adsorption properties and mechanism of geopolymer adsorbents with inherent alkali release for tetracycline. J. Environ. Chem. Eng. 12 (3), 112663 https://doi.org/10.1016/j.jece.2024.112663.
Jusli, E., Nor, H., Jaya, R.P., Haron, Z., 2014. Chemical properties of waste tyre rubber granules. Adv. Mater. Res. 911, 77–81. https://doi.org/10.4028/www.scientific.net/AMR.911.77.
Koble, Robert A., Corrigan, Thomas E., 1952. Adsorption isotherms for pure hvdrocarbons. Ind. Eng. Chem. 44, 383–387. https://doi.org/10.1021/ie50506a049.
Langmuir, I., 1916. The constitution and fundamental properties of solids and liquids. J. Am. Chem. Soc. 38, 2221–2295. https://doi.org/10.2121/ja02268a002.
Li, G., Ben, W., Ye, H., Zhang, D., Qiang, Z., 2018. Performance of ozonation and biological activated carbon in eliminating sulfonamides and sulfonamide-resistant bacteria: a pilot-scale study. Chem. Eng. J. 341, 327–334. https://doi.org/10.1016/j.cej.2018.02.035.
Lian, F., Huang, F., Chen, W., Xing, B., Zhu, L., 2011. Sorption of apolar and polar organic contaminants by waste tire rubber and its chars in single-and bi-solute systems. J. Environ. Pollut. 159, 850–857. https://doi.org/10.1016/J.envol.2011.L.01.002.
Luttah, I., Onunga, D.O., Shikuku, V.O., Otieno, B., Kowenje, C.O., 2023. Removal of endosulfan from water by municipal waste incineration fly ash-based geopolymers: adsorption kinetics, isotherms, and thermodynamics. Front. Environ. Chem. 4, 1164372 https://doi.org/10.3389/fenvc.2023.1164372.
Ndagijimana, P., Liu, X., Yu, G., Wang, Y., 2019. Synthesis of a novel core-shell-structure activated carbon material and its application in sulfamethoxazole adsorption. J. Hazard. Mater. 368, 602–612. https://doi.org/10.1016/j.jhazmat.2019.01.093.
Ngeno, E., Ongulu, R., Orata, F., Matovu, H., Shikuku, V., Onchiri, R., Mayaka, A., Majanga, E., Getenga, Z., Gichumbi, J., Ssebugere, P., 2023. Endocrine disrupting chemicals in wastewater treatment plants in Kenya, East Africa: Concentrations, removal efficiency, mass loading rates and ecological impacts. Environ. Res. 237, 117076 https://doi.org/10.1016/j.envres.2023.117076.
Owino, E.K., Shikuku, V.O., Nyairo, W.N., Kowenje, C.O., Otieno, B., 2023. Valorization of solid waste incinerator fly ash by geopolymer production for removal of anionic bromocresol green dye from water: kinetics, isotherms and thermodynamics studies. Sustain. Chem. Environ. 3, 100026 https://doi.org/10.1016/j.scenv.2023.100026.
Saucier, C., Karthickeyan, P., Ranjithkumar, V., Lima, E.C., dos Reis, G.S., de Brum, I.A. S., 2017. Efficient removal of amoxicillin and paracetamol from aqueous solutions using magnetic activated carbon. Environ. Sci. Pollut. Res. 24, 5918–5932. https://doi.org/10.1007/s11356-016-8304-7.
Shahrokhi-shahraki, R., Benally, C., El-din, M.G., Park, J., 2021. High ef fi ciency removal of heavy metals using tire-derived activated carbon vs commercial activated carbon: insights into the adsorption mechanisms. Chemosphere 264, 128455. https://doi.org/10.1016/j.chemosphere.2020.128455.
Shikuku, V.O., Jemutai-kimosop, S., 2020. Efficient removal of sulfamethoxazole onto sugarcane bagasse-derived biochar: two and three-parameter isotherms, kinetics and thermodynamics. S. Afr. J. Chem. 111, 119. https://doi.org/10.17159/0379-4350/2020/v73a16.
Shikuku, V.O., Tome, S., Hermann, D.T., Tompsett, G.A., Timko, M.T., 2022. Rapid adsorption of cationic methylene blue dye onto volcanic ash - metakaolin based geopolymers. Silicon 14, 9349–9359. https://doi.org/10.1007/s12633-021-01637-9.
Shikuku, V.O., Zanella, R., Bandeira, N., 2017. Single and competitive removal of sulfachloropyridazine and sulfadimethoxine onto natural kaolinite clay: kinetics, isotherms and thermodynamics studies. S. Afr. J. Chem. 120, 126. https://doi.org/10.17159/0379-4350/2017/v70a17.
Shikuku, V.O., Zanella, R., Kowenje, C.O., Donato, Filipe F., Bandeira, Nelson, Prestes, O. D., 2018. Single and Binary Adsorption of sulphonamide antibiotics onto iron-modified clay: linear and nonlinear Isotherms, kinetics, thermodynamics and mechanistic studies. Appl. Water Sci. 8, 175. https://doi.org/10.1007/s13201-018-0825-4.
Sips, R., 2004. On the structure of a catalyst surface. J. Chem. Phys. 490 https://doi.org/10.1063/1.1746922.
Sore, S.O., Messan, A., Prud'homme, E., Escadeillas, G., Tsobnang, F., 2018. Stabilization of compressed earth blocks (CEBs) by geopolymer binder based on local materials from Burkina Faso. Constr. Build. Mater. 165, 333–345. https://doi.org/10.1016/j.conbuildmat.2018.01.051.
Taquieteu, I.K., Tamaguelon, H.D., Shikuku, V., Banenzoué, C., Dina, D.J., 2023. Fixed-Bed Adsorption of an azo dye (Methyl Orange) onto chemically and thermally regenerated activated carbons. J. Chem. vol. 2023 https://doi.org/10.1155/2023/6677710.
Tome, S., Dzoujo, H., Shikuku, V., Nana, A., Annie, M., Rüscher, C., Etame, J., 2023a. Elimination of malachite green from aqueous and saline water by laterite-derived Na-polyferrosialate and polyferrophosphosialate geopolymers: a comparative study. Ceram. Int. https://doi.org/10.1016/j.ceramint.2023.11.252.
Tome, S., Etoh, M.A., Etame, J., Kumar, S., 2020. Improved reactivity of volcanic ash using municipal solid incinerator fly ash for alkali-activated cement synthesis. Waste Biomass-.-. Valoriz. 11, 3035–3044. https://doi.org/10.1007/S12649-019-00604-1.
Tome, S., Hermann, D.T., Shikuku, V.O., Otieno, S., 2021. Synthesis, characterization and application of acid and alkaline activated volcanic ash-based geopolymers for adsorptive remotion of cationic and anionic dyes from water. Ceram. Int. J. 1–9. https://doi.org/10.1016/j.ceramint.2021.04.097.
Tome, S., Shikuku, V., Dzoujo, H., Akiri, S., Annie, M., Rüscher, C., Etame, J., 2023b. Efficient sequestration of malachite green in aqueous solution by laterite - rice husk ash - based alkali - activated materials: parameters and mechanism. Environ. Sci. Pollut. Res. 1–15. https://doi.org/10.1007/s11356-023-27138-3.
Toth, 1971. State equation of the solid-gas interface layers. Acta Chim. Hung. 69, 311–328.
Wang, X., Zhang, Z., Ge, Y., 2022. Oleic acid-tailored geopolymer microspheres with tunable porous structure for enhanced removal from tetracycline in saline water. Sustain. Artic. https://doi.org/10.3390/su14116705.
Xie, Y., Li, Q., Qin, L., Zhou, X., Fan, Y., 2021. Multi-templates surface molecularly imprinted polymer for simultaneous and rapid determination of sulfonamides and quinolones in water: effect of carbon-carbon double bond. Environ. Sci. Pollut. Res.
Yang, Y., Zheng, L., Zhang, T., Yu, H., Zhan, Y., Yang, Y., Zeng, H., Chen, S., Peng, D., 2019. Adsorption behavior and mechanism of sulfonamides on phosphonic chelating cellulose under different pH effects. Bioresour. Technol. 288, 121510 https://doi.org/10.1016/j.biortech.2019.121510.
Zhou, J., Yun, X., Wang, J., Li, Q., Wang, Y., 2021. A review on the ecotoxicological effect of sulphonamides on aquatic organisms. Toxicol. Rep. 9, 534–540. https://doi.org/10.1016/j.toxrep.2022.03.034.
Zhu, Weixiao, Wang, Jianduo, W, Y., W, H., 2018. Study on sulfadimethoxine removal from aqueous solutions by hydrous ferric oxides. Water Sci. Technol. 1136–1142. https://doi.org/10.2166/wst.2016.246.